Efficient visible laser emission of GaN laser diode pumped Pr-doped fluoride scheelite crystals

F. Cornacchia [1,*]**, A. Di Lieto** [1]**, M. Tonelli** [1]**, A. Richter** [2]**, E. Heumann** [2]**, and G. Huber** [2]

[1] *NEST - INFM -CNR, Dipartimento di Fisica dell'Università di Pisa, Largo B. Pontecorvo 3, 56127 Pisa, Italy*

[2] *Institut für Laser-Physik, Universität Hamburg, Luruper Chaussee 149, D-22761 Hamburg, Germany*
Corresponding author: francesco.cornacchia@df.unipi.it

Abstract: In the present work we report on the growth, spectroscopy and laser results of diode pumped Pr-doped $LiYF_4$, $LiLuF_4$ and $LiGdF_4$ fluoride, scheelite-type structure crystals. We measured the polarisation dependent absorption and emission properties as well as the decay time of the $^3P_0$ level. Exploiting the $^3P_2$ absorption around 444 nm, we obtained efficient laser emission under GaN laser diode pumping on several transitions from the green to the near infrared wavelength range.

References and links

1. T. Sandrock, T. Danger, E. Heumann, G. Huber, and B. H. T. Chai, "Efficient Continuous Wave-Laser Emission of Pr^{3+}-Doped Fluorides at Room Temperature," Appl. Phys. B **58**, 149–151 (1994).
2. A. A. Kaminskii, "Visible lasing on five intermultiplet transitions of the ion Pr^{3+}:$LiYF_4$," Sov. Phys. Dokl. **28**, 668 (1983).
3. N. V. Kuleshov, A. S. Shinkevich, V. G. Shcherbitsky, V. P. Mikhailov, T. Danger, T. Sandrock, and G. Huber, "Luminescence and time-resolved excited state absorption measurements in Pr^{3+}-doped $La_2Be_2O_5$ and $KGd(WO_4)_2$ crystals," Opt. Mater. **5**, 111–118 (1996).
4. G. Özen, O. Forte, and B. Di Bartolo, "Downconversion and upconversion dynamics in Pr-doped $Y_3Al_5O_{12}$ crystals," J. Appl. Phys. **97**, 013510 (2005).
5. F. Cornacchia, A. Toncelli, M. Tonelli, R. Simura, A. Yoshikawa, and T. Fukuda, "Spectroscopic properties of $Y_3Sc_2Al_3O_{12}$ (YSAG) single crystals grown by μ-PD technique," Opt. Mater. **30**, 135–138 (2007).
6. T. Danger, A. Bleckmann, and G. Huber, " Stimulated emission and laser action of Pr^{3+}-doped $YAlO_3$," Appl. Phys. B **58**, 413–420 (1994).
7. A. Richter, N. Pavel, E. Heumann, G. Huber, D. Parisi, A. Toncelli, M. Tonelli, A. Diening, and W. Seelert, "Continuous-wave ultraviolet generation at 320 nm by intracavity frequency doubling of red-emitting Praseodymium lasers," Opt. Express **14**, 3282–3287 (2006).
8. F. Cornacchia, A. Richter, E. Heumann, G. Huber, D. Parisi, and M. Tonelli, "Visible laser emission of solid state pumped $LiLuF_4$:Pr^{3+}," Opt. Express **15**, 992–1002 (2007).
9. A. Richter, E. Heumann, G. Huber, V. Ostroumov, and W. Seelert, "Power scaling of semiconductor laser pumped Praseodymium-lasers," Opt. Express **15**, 5172–5178 (2007).
10. A. Richter, E. Heumann, E. Osiac, G. Huber, W. Seelert, and A. Diening, "Diode pumping of a continuous wave Pr^{3+} doped $LiYF_4$ laser," Opt. Lett. **29**, 2638–2640 (2004).
11. P. Camy, J. L. Doualan, R. Moncorgé, J. Bengoechea, and U. Weichmann, "Diode-pumped Pr^{3+}:KY_3F_{10} red laser," Opt. Lett. **32**, 1462–1464 (2007).
12. D. Findlay and R. A. Clay, "The measurement of internal losses in 4-level lasers," Phys. Lett. **20**, 277–278 (1966).

13. J. A. Caird, S. A. Payne, P. R. Staver, A. J. Ramponi, L. L. Chase, and W. F. Krupke, "Quantum electronic properties of the $Na_3Ga_2Li_3F_{12}$:Cr^{3+} laser," IEEE J. Quantum Electron. **24**, 1077–1099 (1988).
14. N. I. Agladze, M. N. Popova, G. N. Zhizhin, V. J. Egorov, and M. A. Petrova, "Isotope structure in optical spectra of $LiYF_4$:Ho^{3+}," Phys. Rev. Lett. **66**, 477–480 (1991).
15. B. H. Chai, J. Lefaucheur, and A. Pham, "Growth of Nd:$GdLiF_4$ single crystals," Proc. SPIE Vol. **1863**, Growth, Characterization, and Applications of Laser Host and Nonlinear Crystals II, B.H. Chai Ed., 9–12 (1993).
16. A. A. Kaminskii, "Laser Crystals. Their Physics and Properties," 2nd edition, Springer Verlag, Heidelberg (1990).
17. A. Richter, "Laser parameters and performance of Pr^{3+}-doped fluorides operating in the visible spectral region," Ph.D. Thesis, University of Hamburg, Cuvillier Verlag, Göttingen (2008).
18. M. Fechner, N.-O. Hansen, A. Richter, E. Heumann, and G. Huber "A compact continuous wave solid-state laser at 320 nm," EPS-QEOD Europhoton Conference, Talk FroA.1, Paris (2008).

1. Introduction

For future lighting applications the development of laser-based devices in the visible spectral region is nowadays one of the major keypoints. Additionally, laser sources emitting in the visible range can be useful in other fields such as data storage, biomedical applications or as calibration stars for astrophysical experiments.

One of the proposed solutions relies in the use of rare earth (RE) doped materials pumped by diode lasers. In this perspective, the most appealing candidate class is represented by Praseodymium doped fluoride crystals. The use of Pr^{3+} is related to the large number of potential laser transitions that are available practically throughout the whole visible range up to the near infrared [1, 2]. In the past years the use of Pr^{3+} as an active ion was limited by the availability of pumping sources in the blue region (practically limited to Ar-ion lasers); nowadays, the development of OPSLs (optically pumped semiconductor lasers) operating at 480 nm and GaN blue laser diodes emitting at 444 nm offers a more efficient pumping scheme leading to an overall improvement of the laser performance.

The choice of the host material is crucial for the optimization of the Pr^{3+} laser performance: usually oxide crystals are characterized by a relatively high energy cut-off of the phonon spectrum which often leads to a strong non-radiative decay of the $^3P_0$ level, quenching the starting laser level [3, 4, 5]. For this reason, so far laser action has been obtained only in a low phonon oxide crystal [6] and the Pr^{3+} laser research is focused on fluorides because of their low phonon energy.

Recently, efficient visible laser emission has been obtained under OPSL pumping with $LiYF_4$ (YLF) and BaY_2F_8 [7], as well as $LiLuF_4$ (LLF) [8, 9] and first diode pumping experiments have been described in Refs. [9, 10, 11].

In the present communication we will focus on our recent results obtained with the class of scheelite materials: the first is the well known YLF, the other two are the isostructural materials LLF and $LiGdF_4$ (GLF). We will compare the differences regarding the crystal growth, the emission and absorption features as well as the dynamical behaviour of the laser emitting level. The core of the paper deals with the laser results in the green, orange, red and near infrared wavelength range under diode pumping: we will present and compare output power and slope efficiencies; finally, the crystals are also characterized using the Findlay-Clay [12] and Caird [13] methods.

1.1. Crystal growth and structural properties

One of the main problems in Pr-doping of materials is related to the large radius of the Pr^{3+} ion; the consequence of the mismatch between Pr^{3+} and the lattice site can result in a low segregation coefficient and, above all, the doping may induce stress, lattice distortions and reduce the overall optical quality. In this regard we analysed three different crystals belonging to the scheelite family: YLF, LLF and GLF. We focussed our attention on this class of crystals be-

cause they feature good thermal conductivity, reasonable high damage threshold and allow blue or UV pumping without colour-center formation or damage. The crystals under investigation crystallize in the scheelite-like structure with four formula units per cell (space group $I4_1/a$ or C_{4h}^6 following the Schönfließ notation) where Pr^{3+} substitutes Y, Lu, or Gd in S_4 symmetry with coordination number equal to 8 [14].

As can be seen from Tab. 1, the three candidates differ in the growth conditions and in the host site size for Pr^{3+}: on one hand, LLF grows in a congruent way enabling the growth of crystals with high optical quality, and, on the other hand, the Lu^{3+} ion is very small compared to the Pr^{3+} ion, resulting in an enhanced possibility for crystal distortions and a low segregation coefficient. On the opposite GLF grows in a highly incongruent manner and only about 10% of the melt is converted into single crystals [15], but the large Gd^{3+} ionic radius allows relatively high Pr^{3+} doping levels in the crystal with reduced amounts of defects. An intermediate situation is represented by YLF, since it grows incongruently (but it is rather easy to obtain high quality samples) and the Y^{3+} radius is large enough for incorporating Pr^{3+} without significant structural distortions [16].

Table 1. Relevant parameters of the crystals under investigation.

crystal (actual doping)	$LiLuF_4:Pr^{3+}$ (0.45%)	$LiYF_4:Pr^{3+}$ (0.65%)	$LiGdF_4:Pr^{3+}$ (0.20%)
melt specification initial composition	congruent LiF 50%, LuF_3 50%	incongruent LiF 53%, YF_3 47%	highly incongruent LiF 68%, GdF_3 32%
T_m (°C)	830	850	750
lattice constants (Å)	a=5.123 c=10.520	a=5.160 c=10.850	a=5.214 c=10.965
ionic radii (Å)	$R_{Lu^{3+}}$=1.12	$R_{Y^{3+}}$=1.16	$R_{Gd^{3+}}$=1.19
	ionic radius $R_{Pr^{3+}}$=1.27 Å		
segregation coefficient k_{eff}	0.1 - 0.2	0.22	0.39
Pr^{3+} density (10^{19} cm^{-3})	6.52	9.00	2.68
length (mm)	9.1	3.4	7.6

All the samples have been grown using the Czochralski method. The Pr^{3+}-doped YLF sample was grown and investigated under Ar^+ laser pumping earlier [1] and the LLF sample was grown at the University of Hamburg [17], while the growth of the GLF single crystal was carried out at the University of Pisa.

The apparatus for the GLF growth consisted of a home-made Czochralski furnace with conventional resistive heating; special care has been devoted to the quality of the vacuum system, which had an ultimate pressure limit better than 10^{-7} mbar, and the growth process was carried out in a high-purity (5N) argon atmosphere. The furnace also provided a device for automatic diameter control.

The GLF sample was grown using LiF and GdF_3 powders (purity 5N) as raw materials for the host and a proper amount of PrF_3 powder. As for the other crystals, the melt temperature for the growth is reported in Tab. 1, together with the lattice parameters and the doping concentration in the crystal. The actual Pr-content has been measured by means of inductively coupled plasma

optical emission spectroscopy (ICPOES). From this data we have been able to estimate the segregation coefficient k_{eff} for LLF, YLF and GLF, confirming the hypotheses derived from the ionic radii of Gd^{3+}, Lu^{3+}, and Y^{3+}.

The single crystalline character of the grown GLF sample was checked using an X-ray Laue technique, that allowed us also to identify the c-crystallographic axis of each crystal and to cut oriented samples. For the stimulated emission experiments, the crystal end faces were polished in laser quality.

1.2. Spectroscopy: experimental set-up and results

In order to ascertain the absence of unwanted impurities and to check the possibility to use the $\approx$444 nm laser emission of GaN laser diodes, we measured the σ and π polarized absorption spectra of the all the samples with a spectrophotometer from the UV to the NIR spectral region (see Fig. 1 for the GLF spectra in the visible region). In Tab. 2, we report the results (peak values and FWHM) in the blue wavelength region: these results show that the 480 nm peak arising from the ground state absorption transition to the $^3P_0$ level perfectly matches the emission wavelength of the OPSL we used in previous experiments [8], while the ground state absorption peak of the $^3P_2$ manifold shows a $\approx$2 nm broad peak around 444 nm suitable for GaN laser diode pumping.

Table 2. Absorption coefficients and linewidths of Pr^{3+}-transitions in the blue wavelength region.

Final state	LiLuF$_4$:Pr^{3+} (0.45%)	LiYF$_4$:Pr^{3+} (0.65%)	LiGdF$_4$:Pr^{3+} (0.20%)
$^3P_0$	α=13.2 cm^{-1}	α=15.4 cm^{-1}	α=4.95 cm^{-1}
($\approx$480 nm)	FWHM=0.50 nm	FWHM=0.60 nm	FWHM=0.50 nm
$^3P_2$	α=6.7 cm^{-1}	α=8.1 cm^{-1}	α=2.08 cm^{-1}
($\approx$444 nm)	FWHM=1.70 nm	FWHM=1.80 nm	FWHM=1.94 nm

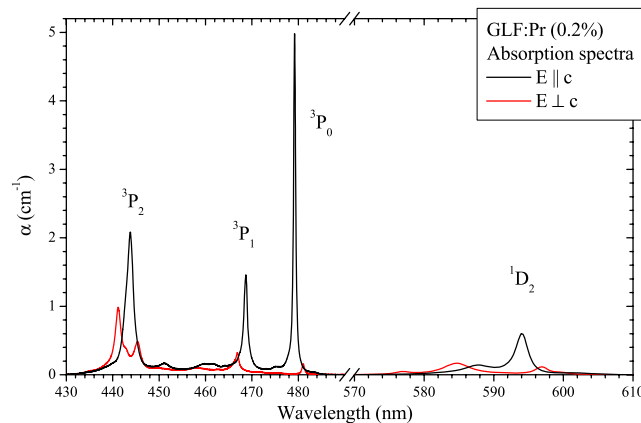To characterize the emission properties of our samples we performed room temperature po-

Fig. 1. Room temperature polarized absorption spectra of GLF:Pr (0.2%).

larized emission measurements in the wavelength range between 460 and 740 nm (in Fig. 2 we report the results for GLF). The excitation source for the emission measurements was a GaN laser diode emitting at 444 nm for the YLF and LLF samples and the 457.9 nm line of an Ar $^+$ laser for GLF. The fluorescence signal, detected perpendicularly to the pump laser direction, was chopped and focused on the input slit of a monochromator, equipped with a polarizer at the entrance in order to perform polarized measurements. For the fluorescence measurements we used a 1200 gr/mm grating blazed at 500 nm. The signal was filtered by proper filters in order to suppress the detection of scattered excitation photons by the sample as much as possible; the fluorescence was detected by a photomultiplier, and the signal fed into pre-amplifiers, processed by a lock-in amplifier and subsequently stored in a PC. The acquired spectra were normalized for the optical response of the system using a black-body source at 3000 K.

To complete the analysis of the visible emission and calculate the emission cross-sections, we measured the $^3P_0$ level room temperature decay time; the set up was similar to that described for the steady state measurements, but in this case the pumping source was a frequency doubled pulsed tunable Ti:Al$_2$O$_3$ (pulse duration ≈ 30 ns) laser in case of GLF or an OPO in case of YLF and LLF. The samples were pumped near an edge and the fluorescence was collected from a thin section (≈ 1 mm) of the sample to observe a uniformly pumped volume and to reduce the influence of radiation trapping effects. Furthermore the power incident on the sample was reduced by means of attenuators to suppress non-linear effects as much as possible. The signal from the photomultiplier was amplified by fast amplifiers and processed by a digital oscilloscope, connected to a PC for storage purposes. The decay curve of the $^3P_0$ state for GLF at the concentration level of 0.2% exhibits a single exponential behaviour that has been fit with τ=43.6 μs. In case of the more concentrated YLF and LLF samples, the decay curves feature non-exponential decay characteristics during the first 20 μs, indicating efficient cross-relaxation processes between close Pr-ions. The effective lifetime has been determined by integrating over the normalized decay curve to be τ=35.7 μs and τ=37.9 μs for YLF and LLF, respectively.

The emission properties and lifetime measurements of Pr^{3+} in YLF and LLF are described in [17] and will not be shown here for the sake of brevity. Thus, Tab. 3 gives the emission cross-sections at the lasing wavelengths calculated by the Füchtbauer-Ladenburg formula.
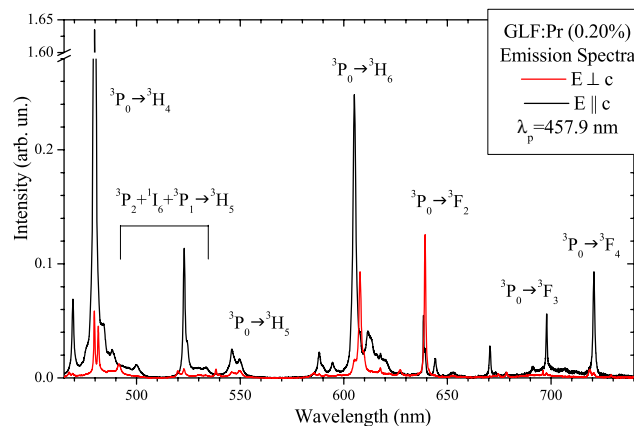

Fig. 2. Room temperature polarized emission spectra of GLF:Pr (0.2%) (λ_p=457.9 nm).

Table 3. Emission wavelengths and cross-sections of Pr^{3+} in LLF, YLF and GLF at the lasing wavelengths.

Transition	λ_{em} (nm)	σ_{em} (10^{-19} cm^2)		
		LLF	YLF	GLF
$^3P_1 \rightarrow{}^3H_5$ $E \parallel c$	$\approx$522	0.3	0.3	0.3
$^3P_0 \rightarrow{}^3H_6$ $E \perp c$	$\approx$607	1.2	1.4	1.3
$^3P_0 \rightarrow{}^3F_2$ $E \perp c$	$\approx$640	2.1	2.2	2.3
$^3P_0 \rightarrow{}^3F_4$ $E \parallel c$	$\approx$720	0.7	0.9	1.6

2. Laser setup and results

The core of this work is represented by the results obtained by GaN diode laser pumping of Pr-doped fluoride scheelite crystals. We used a 3-mirror folded cavity for all the laser experiments, allowing longitudinal pumping of one laser crystal with two laser diodes. The laser diodes provided laser radiation at 444 nm wavelength with $\approx$0.5 W each and $M_x^2=1$ and $M_y^2=3$. Beam shaping of the laser diode radiation was accomplished using a f=4.5 mm collimating lens as well as an anamorphic beam shaping optics, resulting in an almost circular and collimated pump beam. The pump light of each laser diode was focused into the active medium by a f=50 mm lens resulting in an average pump beam diameter of 65 μm inside the medium.

The laser cavity is shown in Fig. 3: the input coupling (IC) mirror had a radius of curvature of 50 mm, the folding mirror was plane and the output coupler (OC) had a radius of curvature of 100 mm. The laser crystal was mounted at the location of the beam waist of the cavity, equal to $\approx$65 μm under optimized length of about 145 mm, depending on the crystal length. The overlap efficiency of the laser and pump mode was less than one because of the different confocal parameters of the pump beam and the resonator mode. For the different laser experiments proper input couplers and folding mirrors have been used, having both high transmission at the 444 nm
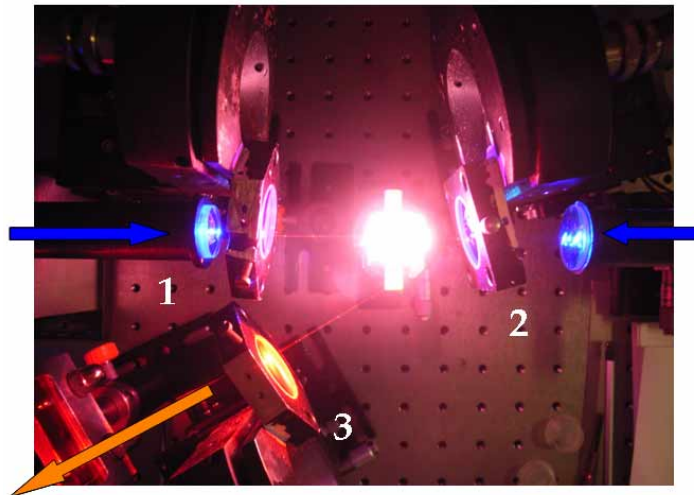

Fig. 3. Picture of the laser set-up. 1 indicates the input coupling mirror, 2 is the plane folding mirror and 3 is the output coupler.

pump wavelength and high reflectivity at the lasing wavelength; in order to perform a detailed analysis of the different laser transitions, several output couplers were used for every experiment. We measured the output spectrum with a Fourier-transform-spectrometer: the repetition of the measurement allowed us to check the spectral stability of the emission. In all the results, we report the slope efficiencies η_{abs}, measured with respect to absorbed power.

2.1. $^3P_0 \rightarrow ^3F_2$ transition: red emission

Table 3 shows the emission cross-sections of Pr^{3+} in the scheelite type host materials. The transition $^3P_0 \rightarrow ^3F_2$ at $\approx$640 nm has an emission cross-section exceeding $2 \cdot 10^{-19}$ cm^2 for all the crystals. Several output couplers with transmissivities of 0.5%, 0.9%, 1.9%, 3.6% and 5.7% were used. The maximum slope efficiency obtained with LLF is 38% using an output coupler transmission of 3.6%: in this case we obtained the best result in terms of output power: 208 mW. The highest slope efficiency for the YLF sample is 41% using T_{oc}=1.9%, while the highest slope efficiency among all hosts has been obtained for the GLF sample: 53% using T_{oc}=5.7%. Considering the higher quantum defect in case of GaN laser diode pumping, these results exceed those reported in Ref. [8] under OPSL pumping at 480 nm directly into the $^3P_0$ energy level. Fig. 4 shows the best laser results in terms of output power for the three samples, while in Tab. 4 we show a summary of output power, thresholds and efficiencies as a function of the output coupler transmissivity.

For the GLF sample, we have also performed the Findlay-Clay [12] and Caird analysis [13]. The two methods return as round-trip loss value respectively 1.5% (Findlay-Clay) and 0.9% (Caird), in good agreement. Furthermore, the maximum achievable slope efficiency was calculated to be 59%, showing that our best result is close to the quantum limit. These results are comparable with that of our previous work [8], where we calculated a loss value of 0.4% for LLF under OPSL pumping, with a mean pump spot size of 28 μm (in contrast to 65 μm and a decreased beam quality factor in case of GaN laser diode pumping); considering the difficulties
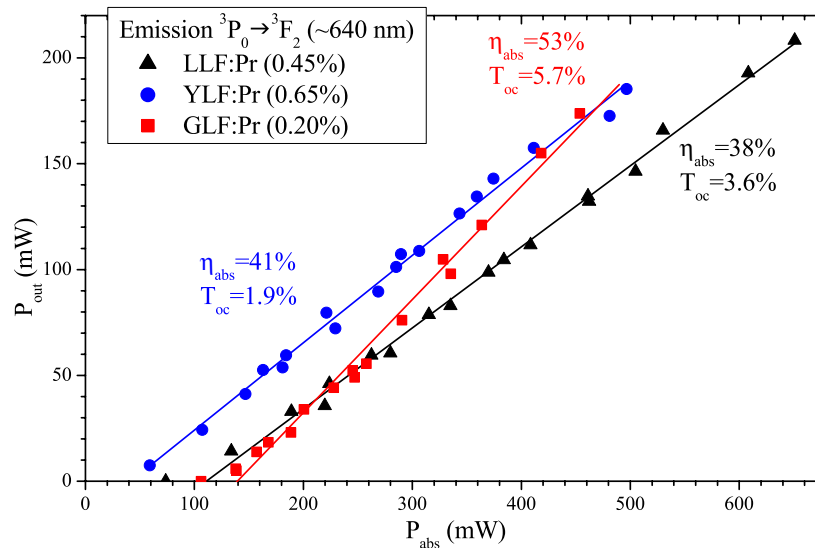

Fig. 4. Best results for the samples under investigation for the $^3P_0 \rightarrow ^3F_2$ transition.

Table 4. Summary of the laser results for the $^3P_0 \rightarrow {}^3F_2$ ($\approx$640 nm) transition for the three samples.

T_{oc} (%)	LLF			YLF			GLF		
	P_{out} (mW)	η_{abs} (%)	P_{thr} (mW)	P_{out} (mW)	η_{abs} (%)	P_{thr} (mW)	P_{out} (mW)	η_{abs} (%)	P_{thr} (mW)
0.5	90	16	71	127	27	33	111	23	37
0.9	134	24	87	159	34	24	129	29	49
1.9	195	35	93	185	41	42	164	37	66
3.6	208	38	111	168	41	84	175	45	106
5.7	–	–	–	135	41	141	174	53	139

of growing GLF, we can emphasize the optical quality of the grown crystal. The round-trip losses for YLF were determined to be 0.5% both for the methods of Findlay-Clay and Caird.

2.2. $^3P_0 \rightarrow {}^3F_4$ transition: deep red emission

As can be seen from Tab. 3, the transition $^3P_0 \rightarrow {}^3F_4$ has emission cross-sections in the range of about $1 \cdot 10^{-19}$ cm^2. The output couplers in use had transmission levels of 0.8%, 1.5%, and 2.8%: in this case all the crystals show the best performance using the last mirror. As can be seen in Fig. 5, the highest output power has been achieved, also in this case, with the LLF, that allow us to reach 149 mW with a slope efficiency of 24% and 133 mW as threshold power. The YLF emitted 129 mW with a threshold of 157 mW and η_{abs}=30%. Even for this transition the best result in terms of slope efficiency is represented by the value of 33% of GLF, that has also the lowest threshold power (82 mW) and a maximum output of 105 mW.

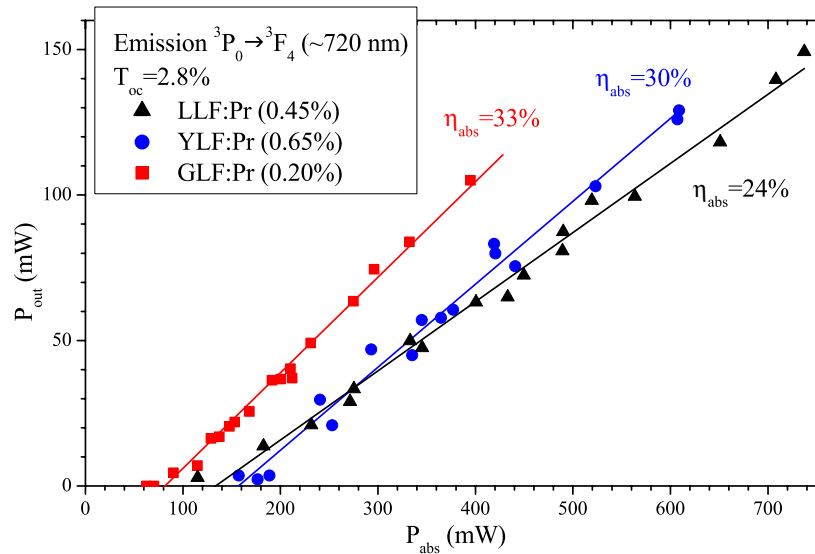The loss analysis for GLF lasing at $\approx$720 nm resulted in 2.6% from the method of Findlay

Fig. 5. Best results for the samples under investigation for the $^3P_0 \rightarrow {}^3F_4$ transition.

and Clay, while the Caird method is in reasonable agreement with the previous 640 nm results indicating about 0.5% for the losses and 39% as maximum attainable slope efficiency, which is comparable to the results for LLF and YLF (0.2% losses and 32% maximum slope efficiency).

2.3. $^3P_0 \to {}^3H_6$ transition: orange emission

The laser performance of the transition $^3P_0 \to {}^3H_6$ has been investigated as well. As shown in Ref. [17], the laser radiation in the orange spectral region suffers from reabsorption due to the $^3H_4 \to {}^1D_2$ transition, resulting in a reduced laser efficiency. Also for this reason, the best results have been achieved with the lowest doping density, i.e. GLF. As can be seen in Fig. 6, using a 3.4% transmission output coupler, we have been able to extract 56 mW with η_{abs}=20% and P_{thr}=128 mW. The lowest threshold was reached for YLF, 105 mW, with P_{out}=42 mW and a slope efficiency of 14%. A similar efficiency, 12%, has been obtained with LLF, that shows 122 mW as threshold power and 36 mW as maximum output power.

2.4. $^3P_1 \to {}^3H_5$ transition: green emission

In the perspective of the development of lighting devices, as well as displays and micro-projectors, the development of an efficient green emitting source will represent a major advancement. Using Pr-based fluoride crystals, it is possible to exploit the $^3P_1 \to {}^3H_5$ transition, emitting around 522 nm. Pumping the $^3P_2$ manifold by means of GaN diodes, fast phonon relaxation populates the metastable level $^3P_0$, but also the $^3P_1$ manifold is thermally populated.

So far we did not obtain laser emission from the LLF sample. With the GLF crystal we achieved a maximum output power of 18 mW with η_{abs}=28% and P_{thr}=288 mW. As can be seen in Fig. 7, the results obtained with YLF are significantly better: the threshold reduces to 205 mW and the slope efficiency increased to 34%, but the most impressive result is represented by the output power that reaches 73 mW, representing, to the best of our knowledge,
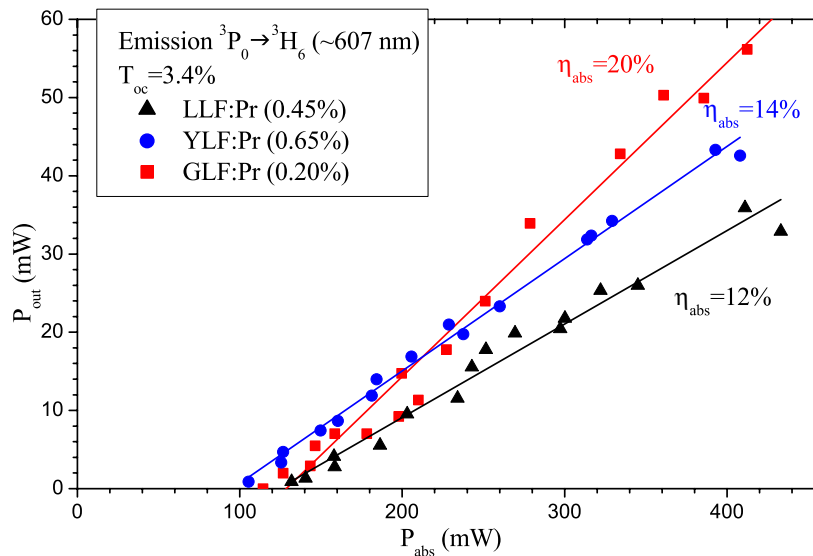

Fig. 6. Best results for the samples under investigation for the $^3P_0 \to {}^3H_6$ transition.
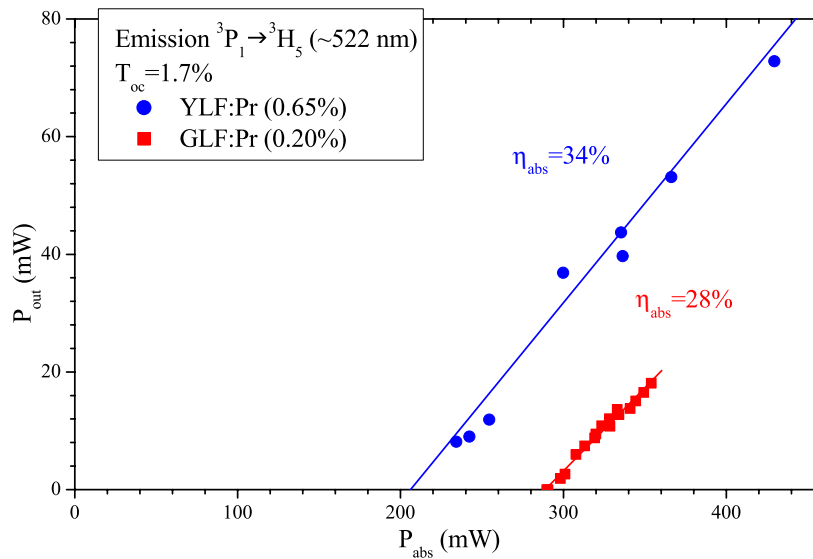
Fig. 7. Best results for the GLF and YLF samples for the $^3P_1 \rightarrow\, ^3H_5$ transition.

the highest value obtained within Pr-doped materials. Findlay-Clay and Caird analysis resulted in round-trip losses of 0.5% and a maximum slope efficiency of 45% for the YLF crystal. For this transition it has been impossible to perform the loss analysis in the case of GLF, since we obtained laser emission only using a 1.33% and a 1.65% transmission OC.

3. Conclusion and further developments

In conclusion, we reported on growth, spectroscopy and diode laser pumped laser experiments with the three Pr^{3+}-doped fluoride scheelite crystals $LiYF_4$, $LiLuF_4$ and $LiGdF_4$. We have obtained efficient continuous-wave laser emission at room temperature for the transitions in the green, orange, red and near-infrared spectral range, with the highest slope efficiencies under GaN diode laser pumping for all transitions, to the best of the authors knowledge. In future we will determine the best host and the optimal Praseodymium content. With respect to the green transition, one of the limiting factors is the amount of absorbed pump power resulting in low Pr laser output powers in the green spectral region. When more powerful GaN diodes will be available on the market, power scaling of all transitions will be possible as well as the improvement of intracavity frequency doubling of the 640 nm [17, 18] and ≈ 522 nm transition.